

Polarization quantum beat spectroscopy of HCF(\tilde{A}^1A'').

I. ^{19}F and ^1H hyperfine structure and Zeeman effect

Haiyan Fan, Ionela Ionescu, Ju Xin,^{a)} and Scott A. Reid^{b)}

Department of Chemistry, Marquette University, Milwaukee, Wisconsin 53201

(Received 2 July 2004; accepted 13 August 2004)

To further investigate the ^{19}F and ^1H nuclear hyperfine structure and Zeeman effect in the simplest singlet carbene, HCF, we recorded polarization quantum beat spectra (QBS) of the pure bending levels 2_0^n with $n=0-7$ and combination bands $1_0^1 2_0^n$ with $n=1-6$ and $2_0^n 3_0^1$ with $n=0-3$ in the HCF $\tilde{A}^1A'' \leftarrow \tilde{X}^1A'$ system. The spectra were measured under jet-cooled conditions using a pulsed discharge source, both at zero field and under application of a weak magnetic field (<30 G). Analysis yielded the nuclear spin-rotation constants C_{aa} and weak field Lande g_{aa} factors. Consistent with a two-state model, the majority of observed vibrational levels exhibit a linear correlation of C_{aa} and g_{aa} , and our analysis yielded effective (\bar{a}) hyperfine constants for the ^{19}F and ^1H nuclei (in MHz) of 728(23) and 55(2), respectively. The latter was determined here owing to the high resolving power of QBS. The vibrational state selectivity of the ^{19}F hyperfine constants is discussed, and we suggest that the underlying Renner-Teller interaction may play an important role. © 2004 American Institute of Physics. [DOI: 10.1063/1.1803529]

I. INTRODUCTION

Carbenes play a role in diverse areas of chemistry, including organic and organometallic reactions,¹⁻⁴ combustion,^{5,6} thermal degradation,⁷⁻¹⁰ and atmospheric and interstellar chemistry.¹¹ As the smallest carbene with a singlet ground state, HCF is a prototype for exploring the spectroscopy, dynamics, and electronic structure of singlet carbenes.¹²⁻³³ The $\tilde{A}^1A'' \leftarrow \tilde{X}^1A'$ system was first observed in absorption by Merer and Travis,²³ who performed rotational analysis for the 2_0^1 and 0_0^0 bands and identified prominent axis-switching transitions arising from the large change in bond angle (opening by $\sim 25^\circ$ in the excited state). The spectroscopy of this system has since been studied in detail by laser induced fluorescence, first by Hirota and co-workers,²⁴⁻²⁸ and more recently by Kable and co-workers^{29,30} and by our group.³¹⁻³³ We have shown that lifetime lengthening occurs for upper state levels with $K'_a \geq 1$ due to the Renner-Teller (RT) interaction,³¹ and we recently reported a detailed spectroscopic study of this system which provided new estimates for the excited state barriers to linearity and dissociation.³³

Less is known about the hyperfine structure or Zeeman effect in this system, which are detailed probes of the electronic structure and important observables for identifying singlet-triplet perturbations. Hirota and co-workers were the first to examine the ^{19}F hyperfine structure and Zeeman effect in the \tilde{A}^1A'' state, using intermodulated fluorescence (IMF) combined with Zeeman tuning.²⁵⁻²⁸ Unperturbed levels in the 0_0^0 band were found to exhibit a small Zeeman

effect arising from interactions with levels of \tilde{X}^1A' , as the two states correlate with a $^1\Delta$ state in the linear configuration.^{26,28} The estimated \tilde{A}^1A'' state Lande g_{aa} factor was $\sim (5-10) \times 10^{-3} \mu_B$.²⁸ In addition, local singlet-triplet perturbations were also identified by their much larger Zeeman effects, up to $1 \mu_B$, although a quantitative analysis was not achieved.^{27,28} The ^{19}F hyperfine constants (C_{aa}) of both \tilde{A}^1A'' [$-7.71(20)$ MHz] and \tilde{X}^1A' [$4.19(14)$ MHz] were determined within a two-state model,²⁸ while hyperfine structure due to the ^1H nucleus was not resolved.

In this paper, we report a study of the HCF $\tilde{A}^1A'' \leftarrow \tilde{X}^1A'$ system using polarization quantum beat spectroscopy.^{32,34,35} The intrinsically high resolution of QBS allows us to resolve both the ^{19}F and ^1H hyperfine structure in the \tilde{A}^1A'' state, which was probed as a function of vibrational level. Zeeman quantum beat spectroscopy was used to determine the weak field Lande g_{aa} factors. The data so obtained have provided detailed information on the electronic structure of this prototypical carbene and the origin of the striking vibrational mode dependence of the ^{19}F spin-rotation constant C_{aa} reported in our preliminary study.³²

II. EXPERIMENTAL SECTION

The apparatus, pulsed discharge nozzle, and data acquisition procedures have previously been described in detail.³¹⁻³⁶ HCF was generated by a pulsed electrical discharge through a $\sim 2\%$ mixture of CH_2F_2 (Aldrich, 99.9%) in argon. The typical backing pressure was ~ 1 bar, and discharge was initiated by a ~ 1 kV pulse of $10-50 \mu\text{s}$ duration, through a current limiting $10 \text{ k}\Omega$ ballast resistor. The timing of laser, nozzle, and discharge firing was controlled by a digital delay generator (Stanford Research Systems DG535), which also generated the variable width gate pulse for our

^{a)}Present address: Department of Physics and Engineering Technologies, Bloomsburg University, Bloomsburg, PA 17815.

^{b)}Author to whom correspondence should be addressed. Electronic mail: scott.reid@mu.edu

high voltage pulser (Directed Energy GRX-1.5K-E). The laser system consisted of an etalon narrowed dye laser (Lambda-Physik Scanmate 2E), pumped by the second or third harmonic of an injection seeded Nd:YAG laser (Continuum Powerlite 7010), where YAG represents yttrium aluminum garnet. For access to wavelengths <430 nm, the fundamental dye output was mixed with the Nd:YAG fundamental in a BBO crystal. The laser beam was not focused, and typical pulse energies were ~ 500 μJ in a ~ 3 mm diameter beam. The laser wavelength was calibrated using optogalvanic spectroscopy in a Fe-Ne or Fe-Ar hollow cathode lamp.

The measurements utilized a mutually orthogonal geometry of laser, molecular beam, and detector, where the laser beam crossed the molecular beam at a distance of ~ 20 nozzle diameters downstream. The laser propagated along the space-fixed Y axis, with the molecular beam oriented along the Z axis, and detector aligned along the X axis. Fluorescence was collected by an $f/2.4$ condenser lens assembly, and filtered via an appropriate long-pass cutoff filter (Corion) prior to striking a photomultiplier tube detector (Oriel) held at typically -600 V.

In acquiring quantum beat spectra, the photomultiplier tube (PMT) signal was terminated into 50 Ω , and digitized by a fast oscilloscope (HP 54521A) at a typical sampling rate of 10^9 s^{-1} . Waveforms averaged over typically 2500 laser shots were collected for parallel and perpendicular laser-detector polarizations. The time-dependent degree of polarization $[P(t)]$ was then calculated at each time point following Eq. (1):

$$P(t) = [I_{\parallel}(t) - I_{\perp}(t)] / [I_{\parallel}(t) + I_{\perp}(t)]. \quad (1)$$

The $P(t)$ thus obtained was Fourier transformed using a fast Fourier transform routine (PSI plot) to yield the quantum beat spectrum. For Zeeman experiments, Earth's magnetic field was nulled and a weak magnetic field (<30 G) was generated along the space fixed X axis using a triaxial Helmholtz coil system (Walker Scientific). In this configuration, the selection rules for Zeeman quantum beats are $\Delta M_F = \pm 2$.

III. RESULTS AND DISCUSSION

We first obtained zero-field quantum beat spectra for ${}^rR_0(J)$ lines of vibronic bands in the \tilde{A}^1A'' state. Consistent with theoretical expectations,³⁷⁻³⁹ the beats were strongest for ${}^rR_0(0)$ lines and decreased in intensity with increasing J . As rotational perturbations were often observed at higher J , analysis was typically limited to ${}^rR_0(0)$ and ${}^rR_0(1)$ lines. Figure 1 displays experimental and simulated quantum beat spectra (QBS) for the ${}^rR_0(0)$ transition of $1_0^1 2_0^3$. The simulation was generated from the time dependent fluorescence intensities for parallel and perpendicular laser-detector polarizations calculated within the density matrix formalism of Huber and co-workers [i.e., Eq. (3) of Ref. 38]. Excellent agreement is observed, and the relative intensities show unambiguously that the ${}^{19}\text{F}$ and ${}^1\text{H}$ constants have the same sign. For comparison, the lower panel of Fig. 1 displays a simulated spectrum for the case where these constants are of

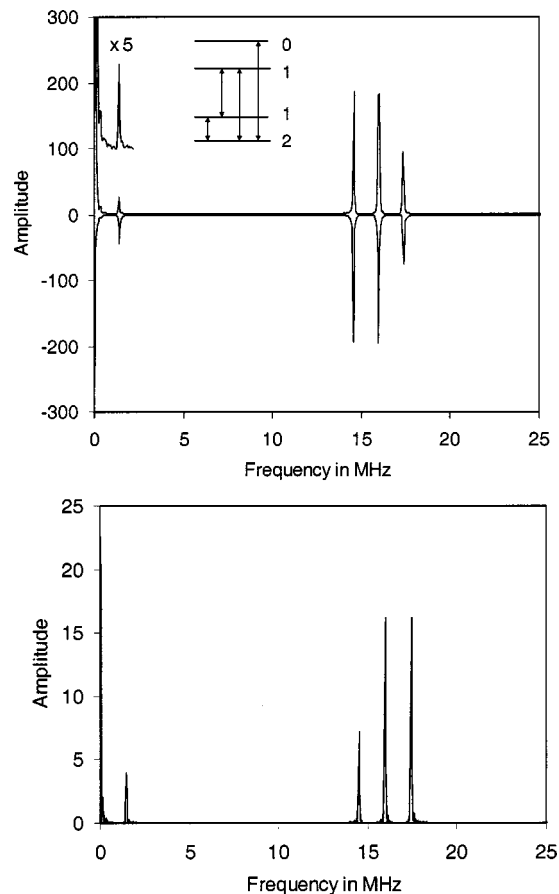


FIG. 1. Upper panel: Experimental (top) and simulated polarization quantum beat spectrum of the ${}^rR_0(0)$ transition of $1^1 2^3$. An expanded ($\times 5$) view of the low frequency region of the experimental spectrum is shown to demonstrate the noise level, and the beat assignments are referenced to the energy level diagram given in the upper panel, where the labels indicate the F quantum number. Lower panel: Simulated quantum beat spectrum for the case where the ${}^{19}\text{F}$ and ${}^1\text{H}$ nuclear spin-rotation hyperfine constants (C_{aa}) are of opposite sign.

opposite sign. Note that the small ${}^1\text{H}$ splittings, which were not resolved in previous IMF studies, are identified here through the high resolving power of QBS.

The dominant contribution to the hyperfine structure in the \tilde{A}^1A'' state of HCF is the nuclear spin-rotation interaction, with Hamiltonian given by²⁸

$$H_{nsr} = C_{aa}I_aJ_a + C_{bb}I_bJ_b + C_{cc}I_cJ_c. \quad (2)$$

Here $C_{aa} \gg C_{bb}, C_{cc}$, and therefore C_{bb} and C_{cc} were set to zero in our analysis, their expected magnitude being less than our experimental uncertainty. The ${}^{19}\text{F}$ and ${}^1\text{H}$ C_{aa} hyperfine constants were obtained by fitting the observed zero-field beat frequencies to values calculated by diagonalizing the Hamiltonian matrix in the basis: $\mathbf{F}_1 = \mathbf{J} + \mathbf{I}_F$, $\mathbf{F} = \mathbf{F}_1 + \mathbf{I}_H$.²⁸ While quantum beat spectra were obtained for rotational lines in ~ 20 vibronic levels, only those levels that were identified as unperturbed on the basis of spectroscopic and lifetime analysis³¹⁻³³ are included in Fig. 2, which displays the derived C_{aa} constants for ${}^{19}\text{F}$ (upper panel) and ${}^1\text{H}$, plotted as a function of \tilde{A}^1A'' state vibrational energy. Note that the error bars are smaller than the symbol size.

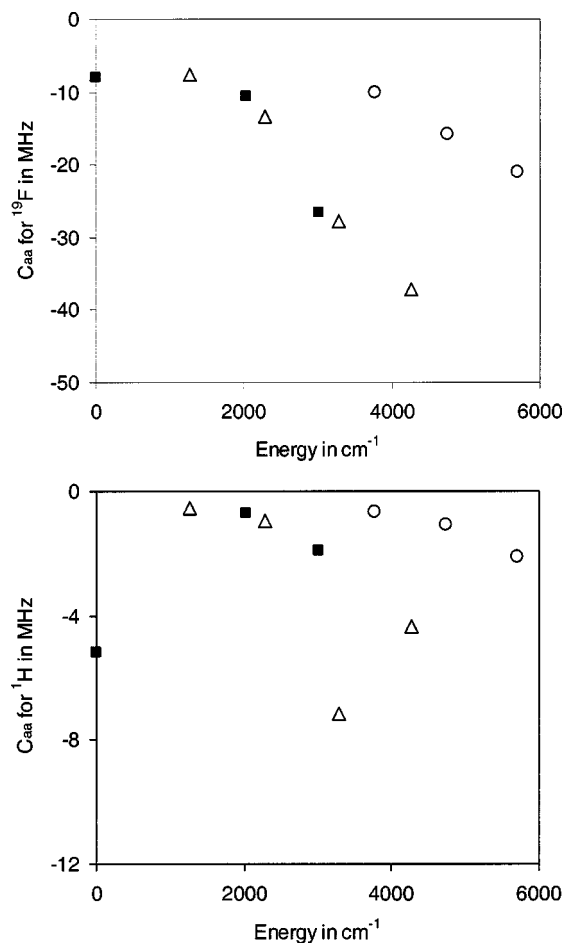


FIG. 2. Energy dependence of the measured ^{19}F (upper panel) and ^1H nuclear spin-rotation constants. $\blacksquare=2^n$, $\triangle=2^n 3^1$, $\circ=1^1 2^n$. Note that the error bars are smaller than the symbol size.

The hyperfine constants display a pronounced energy and vibrational state specificity which can be largely traced to variations in the A rotational constant. Neglecting small terms arising from closed shell electrons and other nuclei, and assuming that only \tilde{X}^1A' state levels contribute to the sum,²⁸ the nuclear spin/overall rotation constant C_{aa} can be expressed as^{28,40}

$$C_{aa}(v') = -4 \sum_{v''} \frac{\langle \tilde{A}, v' | a L_a | \tilde{X}, v'' \rangle \langle \tilde{X}, v'' | A L_a | \tilde{A}, v' \rangle}{E_{v''} - E_{v'}}. \quad (3)$$

In Eq. (3) A is the a -axis rotational constant, a is the nuclear spin/electron orbital coupling constant, v is a generic vibrational state label, and L_a is the orbital angular momentum operator. To approximately separate out the dependence on A , we plot in Fig. 3 the hyperfine constants vs quanta of bending excitation, noting that levels containing equal quanta of bend display similar A constants.³³ The upper panel of this plot clearly shows the trend described in our preliminary report,³² namely, larger $C_{aa}(^{19}\text{F})$ constants for levels containing C-F stretching excitation. We suggested previously that this trend may be due to an increase in the a hyperfine constant for the ^{19}F nucleus.³² That hypothesis was tested here by combining hyperfine and Zeeman measurements.

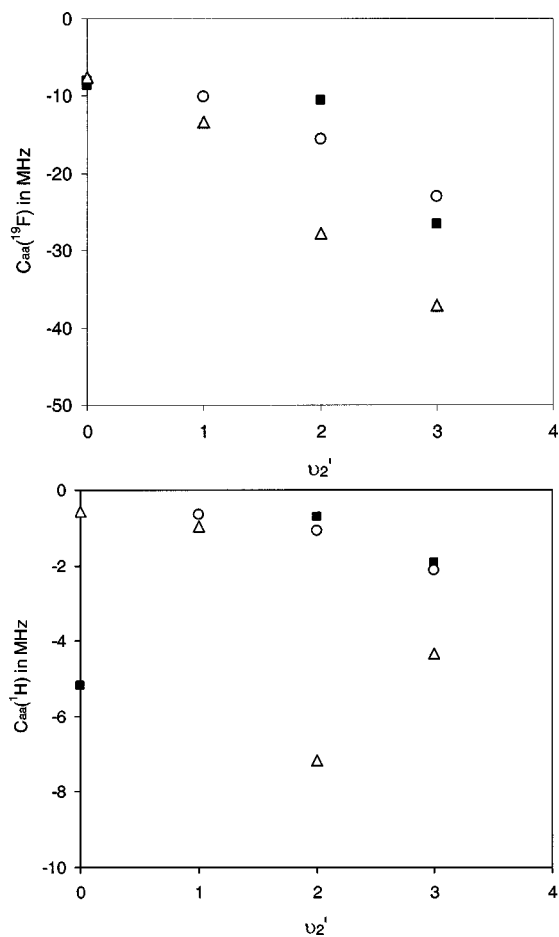


FIG. 3. Dependence of the ^{19}F (upper panel) and ^1H nuclear spin-rotation constants on quanta of v_2' . $\blacksquare=2^n$, $\triangle=2^n 3^1$, $\circ=1^1 2^n$. Note that the error bars are smaller than the symbol size.

When Eq. (3) is valid, the excited state Landé g_{aa} factor can be expressed as^{28,40}

$$g_{aa}(v') = 4 \sum_{v''} \frac{\langle \tilde{A}, v' | L_a | \tilde{X}, v'' \rangle \langle \tilde{X}, v'' | A L_a | \tilde{A}, v' \rangle}{E_{v''} - E_{v'}}. \quad (4)$$

Combining Eqs. (3) and (4), and assuming that the a constant is independent of vibrational level, we obtain⁴⁰

$$-C_{aa}(v')/g_{aa}(v') \cong \bar{a}, \quad (5)$$

where \bar{a} is the effective (average) hyperfine constant of \tilde{X}^1A' and \tilde{A}^1A'' . Equation (5) shows that a plot of C_{aa} vs g_{aa} should be linear, with zero intercept and slope equal to $-\bar{a}$. We derived the $g_{aa}(v')$ via global fits of the Zeeman data for each vibrational level, with the hyperfine constants fixed to the values determined from analysis of the zero-field data. In practice, letting the hyperfine parameters float as variables in the Zeeman analysis returned values that were equal to those determined from the zero-field spectra to within the uncertainty of the fit. The observed frequencies were initially fit via a least-squares routine to values calculated by diagonalizing the Zeeman matrix at each field strength value, which

TABLE I. Hyperfine and Zeeman parameters for HCF(\bar{A}^1A'').

Level	T (cm^{-1})	A (cm^{-1})	$C_{aa}({}^{19}\text{F})$ (MHz)	$C_{aa}({}^1\text{H})$ (MHz)	g_{aa}
0^0	17282.027(16) ^a	25.686(8)	-8.04(27)	-5.19(33)	0.095(6)
3^1	18551.784(63)	25.80(12)	-7.63(7)	-0.55(8)	0.011(1)
2^2	19313.785(37)	32.462(69)	-10.56(6)	-0.70(8)	0.018(2)
2^13^1	19567.057(68)	29.05(10)	-13.37(4)	-0.96(5)	0.019(2)
2^3	20305.737(60)	38.919(89)	-26.55(2)	-1.92(2)	0.034(2)
2^23^1	20562.330(62)	35.54(9)	-27.75(2)	-7.17(2)	0.074(3)
1^12^1	21051.100(51)	26.445(72)	-10.02(6)	-0.64(6)	0.014(1)
2^33^1	21545.38(13)	41.12(22)	-37.15(9)	-4.34(12)	0.070(3)
1^12^2	22024.298(82)	29.94(12)	-15.74(17)	-1.09(18)	0.021(3)
1^12^3	22981.395(77)	37.32(14)	-21.02(3)	-2.12(3)	0.030(2)

^aThree standard errors given in parentheses.

yielded Landé g_F factors for each level. These were consistent in all cases with the weak field vector coupling model in the basis: $\mathbf{F}_1 = \mathbf{J}_1 + \mathbf{I}_F$, $\mathbf{F} = \mathbf{F}_1 + \mathbf{I}_H$. Using a second least-squares program, we then conducted a single-parameter fit of the data to determine g_{aa} for each vibrational level. The values derived for unperturbed levels are given together with the hyperfine constants in Table I. Note that, due to the high resolving power of QBS, even small g_{aa} factors on the order of ~ 0.01 can be determined to within 10%.

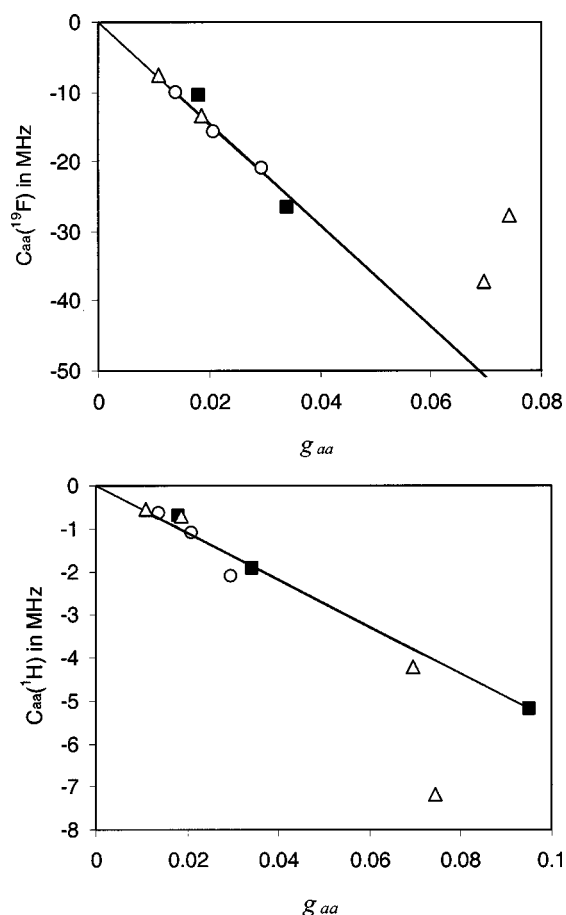


FIG. 4. Dependence of the ${}^{19}\text{F}$ (upper panel) and ${}^1\text{H}$ nuclear spin-rotation constants on Landé g_{aa} factor. Linear fits (lines) are also shown, as described in the text. $\blacksquare = 2^n$, $\triangle = 2^n 3^1$, $\circ = 1^1 2^n$. Note that the error bars are smaller than the symbol size.

Figure 4 displays plots of $C_{aa}({}^{19}\text{F})$ [upper panel] and $C_{aa}({}^1\text{H})$ vs g_{aa} . Consistent with Eqs. (3)–(5), the majority of data in both plots fall on a straight line passing through the origin. The exceptions are the higher members of $2^n 3^1$, and we comment on this observation below. Linear fits of the data for the rest of the vibrational levels are shown in Fig. 4, the slopes of which give \bar{a} constants of 728(23) and 55(2) MHz for ${}^{19}\text{F}$ and ${}^1\text{H}$, respectively. The former is consistent with the value of 737 MHz estimated by Suzuki and Hirota for the 0_0^0 band,²⁸ and may be compared with values of 758.06(23) MHz for the ${}^1\Delta$ state of the isoelectronic NF radical,⁴¹ and 705.82(41) MHz for the ${}^2\Pi$ state of the CF radical.⁴² Comparing \bar{a} with the atomic value for fluorine,⁴³ we derive a spin density of $\sim 17\%$ at the ${}^{19}\text{F}$ nucleus. The interpretation of the proton hyperfine constant is not as straightforward;⁴⁴ however, we note that the derived value is similar to that (54.2 MHz) found for the ${}^2\Pi$ state of the CH radical.⁴⁵

The strong correlation observed in Fig. 4 indicates that the a hyperfine constant in the \bar{A}^1A'' state is independent of vibrational level. Therefore, the observed vibrational selectivity (Fig. 3) must have another origin. Using effective rotational (\bar{A}) and hyperfine (\bar{a}) constants,^{28,32,40} Eq. (3) can be rewritten as

$$C_{aa}(v') = -4\bar{a}\bar{A} \sum_{v''} \frac{\langle \bar{A}, v' | L_a | \bar{X}, v'' \rangle^2}{E_{v'} - E_{v''}}. \quad (6)$$

For comparison with our previous report,³² we show in Fig. 5 a plot of the C_{aa} constants versus effective rotational constant \bar{A} ,⁴⁶ incorporating new data for the $1^1 2^n$ progression. [Here we added the two constants observed for the (Renner-Teller) split $K_a = 1$ subband of 2^1 .] The ${}^{19}\text{F}$ constants clearly fall on two different lines of essentially identical slope. With the exception of $1^1 2^2$, all combination states lie on one line, with the pure bending states on another, suggesting that the latter may be the unique set of levels. Although the observed linear behavior appears to validate the use of Eq. (6), this treatment will break down in cases where near resonances occur with high vibrational levels of \bar{X}^1A' , as the sign of terms in the sum can be positive or negative depending on the relative ordering of the levels. This explains why small hyperfine constants and Zeeman effects are observed for strongly RT perturbed levels,³³ as we show in a detailed

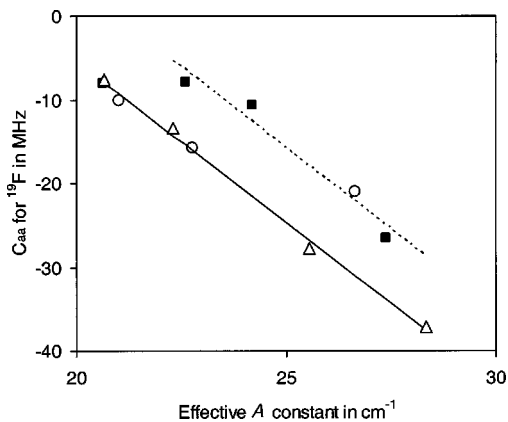


FIG. 5. Dependence of the ^{19}F (upper panel) nuclear spin-rotation constant on effective A rotational constant. Linear fits (lines) are shown to guide the eye. $\blacksquare = 2^n$, $\triangle = 2^n 3^1$, $\circ = 1^1 2^n$. Note that the error bars are smaller than the symbol size.

analysis of 2^4 which forms the basis of the second paper in this series. Thus, the trend observed in Fig. 5 may reflect the underlying RT interaction, although further work is needed to clarify this issue.

We note that the $2^2 3^1$ and $2^3 3^1$ levels show a *larger* Zeeman effect than expected based upon the trend observed for the other levels (Fig. 4). Consistent with previous work,^{25–28} we find, in addition to lifetime lengthening,^{31,33} large Zeeman (and hyperfine) splittings associated with singlet-triplet perturbations in this system.³³ However, the levels probed in $2^2 3^1$ and $2^3 3^1$ were not identified as perturbed on the basis of our spectroscopic analysis³³ or lifetime measurements, and the ^{19}F hyperfine constants of these levels follow the trend of the other members of this progression (Fig. 5). Thus, at the present time this observation remains unexplained. We plan to address this question and probe in further detail the vibrational state dependence of the hyperfine parameters in this system by conducting similar experiments on DCF. This will require a detailed spectroscopic study similar to that recently reported for HCF,³³ which is currently underway in our laboratory.

ACKNOWLEDGMENTS

We gratefully acknowledge the donors of the Petroleum Research Fund of the American Chemical Society and the National Science Foundation (Grant No. CHE-0353596) for support of this research.

¹ *Carbenes*, edited by R. A. Moss and M. Jones, Jr., *Reactive Intermediates in Organic Chemistry Series Vol. I* (Wiley-Interscience, New York, 1973); *Reactive Intermediates in Organic Chemistry Series Vol. II* (Wiley-Interscience, New York, 1975).

² W. Kirmse, *Carbene Chemistry*, 2nd ed. (Academic, New York, 1971).

³ J. C. Sciano, *Handbook of Organic Photochemistry* (CRC Press, Boca Raton, FL, 1989), Vol. 2, Chap. 9.

⁴ F. A. Carey and R. J. Sundberg, *Advanced Organic Chemistry*, 3rd ed. (Plenum, New York, 1990), Pt. 3.

⁵ U. E. Weirsum and L. W. Jenneskens, in *Gas Phase Reactions in Organic Synthesis*, edited by Y. Vallée (Gordon and Breach, Australia, 1997).

- ⁶ A. M. Dean and J. W. Bozzelli, in *Gas-phase Combustion Chemistry*, edited by W. C. Gardiner, Jr., (Springer, New York, 2000), Chap. 2.
- ⁷ G. B. Bacskay, M. Martoprawiro, and J. C. Mackie, *Chem. Phys. Lett.* **290**, 391 (1998).
- ⁸ K. Sendt, E. Ikeda, G. B. Bacskay, and J. C. Mackie, *J. Phys. Chem. A* **103**, 1054 (1999).
- ⁹ M. Martoprawiro, G. B. Bacskay, and J. C. Mackie, *J. Phys. Chem. A* **103**, 3923 (1999).
- ¹⁰ K. Sendt, G. B. Bacskay, and J. C. Mackie, *J. Phys. Chem. A* **104**, 1861 (2000).
- ¹¹ R. P. Wayne, *Chemistry of Atmospheres* (Oxford University Press, Oxford, 1991), Chap. 8, and references therein.
- ¹² E. A. Carter and W. A. Goddard III, *J. Chem. Phys.* **88**, 1752 (1988).
- ¹³ C. W. Bauschlicher, Jr., H. F. Schaefer III, and P. S. Bagus, *J. Am. Chem. Soc.* **99**, 7106 (1977).
- ¹⁴ G. E. Scseria, M. Durán, R. G. A. R. MacLagan, and H. F. Schaefer III, *J. Am. Chem. Soc.* **108**, 3248 (1986).
- ¹⁵ K. K. Irikura, W. A. Goddard III, and J. L. Beauchamp, *J. Am. Chem. Soc.* **114**, 48 (1992).
- ¹⁶ E. A. Carter and W. A. Goddard III, *J. Phys. Chem.* **91**, 4651 (1987).
- ¹⁷ S. K. Shin, W. A. Goddard III, and J. L. Beauchamp, *J. Chem. Phys.* **93**, 4986 (1990).
- ¹⁸ G. L. Gutsev and T. Ziegler, *J. Phys. Chem.* **95**, 7220 (1991).
- ¹⁹ N. Russo, E. Sicilia, and M. Toscano, *J. Chem. Phys.* **97**, 5031 (1992).
- ²⁰ B. Weis, P. Rosmus, K. Yamashita, and K. Morokuma, *J. Chem. Phys.* **92**, 6635 (1990).
- ²¹ T. W. Schmidt, G. B. Bacskay, and S. H. Kable, *Chem. Phys. Lett.* **292**, 80 (1998).
- ²² R. I. Patel, G. W. Stewart, K. Casleton, J. L. Gole, and J. R. Lombardi, *Chem. Phys.* **52**, 461 (1980).
- ²³ A. J. Merer and D. N. Travis, *Can. J. Phys.* **44**, 1541 (1966).
- ²⁴ M. Kakimoto, S. Saito, and E. Hirota, *J. Mol. Spectrosc.* **88**, 300 (1981).
- ²⁵ T. Suzuki, S. Saito, and E. Hirota, *J. Mol. Spectrosc.* **90**, 447 (1981).
- ²⁶ R. J. Butcher, S. Saito, and E. Hirota, *J. Chem. Phys.* **80**, 4000 (1984).
- ²⁷ T. Suzuki, S. Saito, and E. Hirota, *Can. J. Phys.* **62**, 1328 (1984).
- ²⁸ T. Suzuki and E. Hirota, *J. Chem. Phys.* **85**, 5541 (1986).
- ²⁹ T. W. Schmidt, G. B. Bacskay, and S. H. Kable, *J. Chem. Phys.* **110**, 11277 (1999).
- ³⁰ K. Nauta, J. S. Guss, N. L. Owens, and S. H. Kable, *J. Chem. Phys.* **120**, 3517 (2004).
- ³¹ H. Fan, I. Ionescu, C. Annesley, and S. A. Reid, *Chem. Phys. Lett.* **378**, 548 (2003).
- ³² I. Ionescu, H. Fan, C. Annesley, J. Xin, and S. A. Reid, *J. Chem. Phys.* **120**, 1164 (2004).
- ³³ H. Fan, I. Ionescu, C. Annesley, J. Cummins, M. Bowers, J. Xin, and S. A. Reid, *J. Phys. Chem. A* **108**, 3732 (2004).
- ³⁴ J. Xin, I. Ionescu, D. Kuffel, and S. A. Reid, *Chem. Phys.* **291**, 61 (2003).
- ³⁵ J. Xin, I. Ionescu, H. Fan, and S. A. Reid, *Rec. Res. Develop. Chem. Phys.* **5**, 211 (2004).
- ³⁶ J. Xin, H. Fan, I. Ionescu, C. Annesley, and S. A. Reid, *J. Mol. Spectrosc.* **219**, 37 (2003).
- ³⁷ M. Dubs, J. Mühlbach, H. Bitto, P. Schmidt, and J. R. Huber, *J. Chem. Phys.* **83**, 3755 (1985).
- ³⁸ M. Dubs, P. Schmidt, and J. R. Huber, *J. Chem. Phys.* **85**, 6335 (1986).
- ³⁹ H. Bitto, M. P. Docker, P. Schmidt, and J. R. Huber, *J. Chem. Phys.* **92**, 187 (1990).
- ⁴⁰ C. H. Townes and A. L. Schawlow, *Microwave Spectroscopy* (McGraw-Hill, New York, 1955), Chap. 8.
- ⁴¹ P. B. Davies, P. A. Hamilton, and M. Okumura, *J. Chem. Phys.* **75**, 4294 (1981).
- ⁴² S. Saito, Y. Endo, M. Takami, and E. Hirota, *J. Chem. Phys.* **78**, 116 (1983).
- ⁴³ J. S. M. Harvey, *Proc. R. Soc. London, Ser. A* **285**, 581 (1965).
- ⁴⁴ *High Resolution Spectroscopy of Transient Molecules*, edited by E. Hirota (Springer, Berlin, 1985), Chap. 4.
- ⁴⁵ M. Bogey, C. Demuynck, and J. L. Destombes, *Chem. Phys. Lett.* **100**, 105 (1983).
- ⁴⁶ The effective rotational constant is defined as $[A(\bar{A}^1 A'', v') + A(\bar{X}^1 A', v'' = 0)]/2$.